Appendix B

Microwave Sintering of Hybrid Composites

B1 Introduction

Additional work carried out on the microwave sintering of hybrid composites using microwave sintering is provided in this appendix. Two hybrid composite formulations were investigated: i) Mg reinforced with 9 vol.% of micron (25 μm) and 1 vol.% of nano (50 nm) SiC[1] and ii) Mg reinforced with 4 – 4.5 vol.% of submicron (0.3 μm) and 0.5 - 1 vol.% of nano (50 nm) Al_2O_3[2].

B2 Hybrid Mg/SiC Composites

B2.1 Results and Discussion

B2.1.1 Density and Porosity Measurements

Results of density and porosity measurements revealed that near dense monolithic and composite materials can be obtained using the fabrication methodology adopted in this study. The highest porosity was exhibited by hybrid composite samples and was limited to 1.75% (see Table B1).

B2.1.2 Microstructural Characterization

Microstructural characterization of Mg10%μm-SiC revealed minimal porosity, fairly uniform distribution of SiC particulates and good SiC-Mg interfacial integrity (see Fig. B1a and b) which was assessed in terms of the presence of microvoids and/or debonding.

[1] The result for Mg/SiC hybrid composite has been published in **Solid State Phenomena** Vol. 111: 91-94. 2006.

[2] The result for Mg/Al_2O_3 hybrid composite has been published in **Journal of Materials Science** Vol. 40: 3395-3402. 2005.

For Mg1%nm-SiC composite, micrographs indicate a continuous network of nano-sized SiC particulates decorating the particle boundaries of the matrix and evidence of inter-particle porosity (see Fig. B1c).

Table B1 Results of density and porosity measurements.

Materials	SiC Reinforcement (Vol%)		Experimental Density	Porosity
	25μm	50nm	(g/cm^3)	(%)
Pure Mg	-	-	1.731 ± 0.007	0.52
Mg1%nm-SiC	-	1.0	1.753 ± 0.002	0.11
Mg10%μm-SiC	10.0	-	1.865 ± 0.004	1.22
Mg Hybrid	9.0	1.0	1.855 ± 0.006	1.75

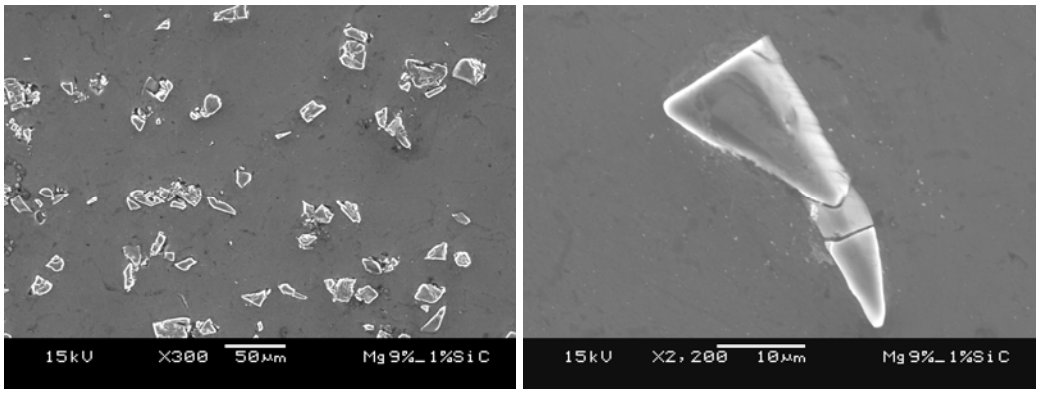

(a) (b)

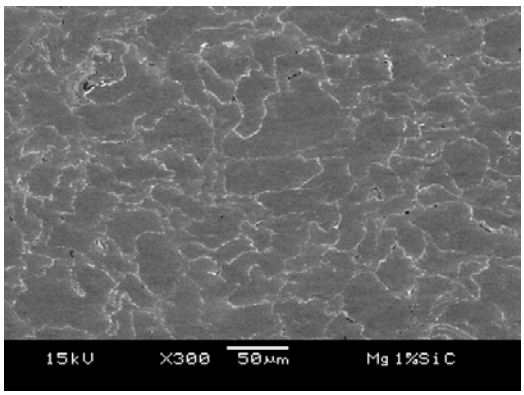

(c)

Figure B1 Representative micrographs showing: (a) distribution of micron size SiC particulates in the matrix, (b) interfacial integrity between micron size SiC particulates and matrix and (c) continuous network of nano-size SiC particulates decorating the particle boundaries of the matrix.

B2.1.3 CTE and XRD Analysis

Thermal mechanical analysis revealed a reduction of ~14% in the average CTE values of the magnesium matrix with the addition of hybrid reinforcement (see Table B2). The decrease in CTE values can be attributed to: (a) lower CTE of SiC (4.3 x 10^{-6} / K^{-1} for SiC [1] compared to 29.1 x 10^{-6} / K^{-1} for Mg) (b) good interfacial integrity between reinforcements and the matrix and (c) the ability of the reinforcements to effectively constrain the expansion of the matrix. Results of X-ray diffraction studies shown in Table B2 confirmed the presence of Mg and SiC phases in composite samples.

Table B2 Results of CTE and XRD analysis.

Materials	**SiC Reinforcement (Vol%)**		**CTE**	**No of matching peaks**	
	25μm	**50nm**	**x10^{-6} K^{-1}**	**Mg**	**SiC**
Pure Mg	-	-	29.1 ± 1.2	6[1]	-
Mg1%nm-SiC	-	1.0	28.1 ± 0.9	6[2]	-
Mg10%μm-SiC	10.0	-	25.6 ± 1.9	8[2]	2[1]
Mg Hybrid	9.0	1.0	24.9 ± 0.5	10[2]	3[2]

[ ] represents the main peaks matched

B2.1.4 Mechanical Characterization

The results of mechanical characterization revealed an improvement in microhardness and 0.2%YS (see Table B3) in the case of composite samples. The ductility of the composites decreased with the addition of reinforcement except in the case of Mg reinforced with 1vol% of nano-size SiC.

The increase in microhardness (see Table B3) of magnesium matrix in the case of composite materials can be attributed primarily to the: (a) presence of harder reinforcements in the matrix and (b) higher constraint to the localized matrix deformation due to the presence of the reinforcements. These results are also consistent with the

observation of other researchers [2-5]. Hybrid composites exhibited the best microhardness and this can be attributed to the superior ability of hybrid (length scale difference) reinforcements when compared to the single length scale reinforcement.

Tensile testing revealed that the presence of nano-size SiC reinforcement in Mg1%nm-SiC lead to a greater improvement in the 0.2%YS when compared to Mg10%μm-SiC. The UTS and ductility values were observed to be higher in Mg1%nm-SiC when compared to Mg10%μm-SiC. The hybrid composite displayed comparable 0.2%YS value with Mg1%nm-SiC. UTS was reduced but still remained higher than pure magnesium and Mg10%μm-SiC.

Table B3 Results of hardness and tensile properties.

Materials	Microhardness (HV)	0.2% YS (MPa)	UTS (MPa)	Ductility (%)
Pure Mg	38.6 ± 1.5	125 ± 15	172 ± 12	5.8 ± 0.9
Mg1%nm-SiC	43.2 ± 2.0	157 ± 22	203 ± 22	7.6 ± 1.5
Mg10%μm-SiC	44.3 ± 0.5	140 ± 2	165 ± 2	1.5 ± 0.8
Mg Hybrid	50.9 ± 1.0	156 ± 7	185 ± 11	0.6 ± 0.1

The increase in yield strength of the composite samples can be attributed to: (a) increase in dislocation density and the formation of internal stresses due to different thermal expansion mismatch between reinforcements and the matrix [1] and (b) effective transfer of applied tensile load to the well bonded uniformly distributed reinforcements [1]. The decrease in UTS and ductility with the addition of micron-size SiC particulates can be attributed to the reduced cavitation resistance of magnesium matrix due to the combined presence of porosity and micron-size SiC particulates [3, 6]. The increase in ductility in the case of Mg1%nm-SiC can be attributed to the ability of nanometric size

SiC particulates to activate the non-basal plane slip planes [7]. Similar increase in ductility has also been observed in the case of Ti [8], CNT [9] and nano-Al_2O_3 [10] reinforced Mg samples.

B2.2 Conclusions

(1) Powder metallurgy technique coupled with microwave assisted rapid sintering and hot extrusion can be used successfully to synthesize monolithic Mg and conventional and hybrid composites.

(2) Thermal stability, hardness and 0.2%YS of magnesium matrix was enhanced with the addition of SiC particulates irrespective of its different length scales.

(3) Mg hybrid composite consisting of SiC particulates of two different length scales exhibited superior thermal stability and hardness when compared to singularly reinforced composites. Yield strength of Mg hybrid composite remained comparable to that of Mg1%nm-SiC.

B3 Hybrid Mg/Al_2O_3 Composites

B3.1 Results and Discussion

B3.1.1 Synthesis of Mg and Mg/Al_2O_3 Hybrid Composites

The synthesis of hybrid magnesium composites containing reinforcement of two different sizes was successfully achieved using two-directional microwave assisted sintering followed by hot extrusion. The results of macrostructural characterization on the extruded Mg and Mg/Al_2O_3 samples revealed the absence of macro defects. The outer surface was smooth and free of circumferential cracks. The results of density and porosity measurements indicate that near dense monolithic and composite formulations can be achieved using the fabrication methodology used in the present study (see Table B4).

Table B4 Results of density and porosity measurements.

Materials	Reinforcement (Vol. %)		Theoretical Density(ρ) (g/cm^3)	Experimental Density(ρ) (g/cm^3)	Porosity (%)
	50-nm	0.3-μm			
Mg	-	-	1.740	1.738 ± 0.001	0.07
Mg/Al_2O_3	0.5	4.5	1.851	1.840 ± 0.003	0.58
Mg/Al_2O_3	0.75	4.25	1.851	1.837 ± 0.005	0.75
Mg/Al_2O_3	1.0	4.0	1.851	1.831 ± 0.005	1.04

B3.1.2 Microstructure Characterization

Microstructural characterization of the extruded Mg and Mg/Al_2O_3 composites revealed near equiaxed grain shape and the presence of submicron size Al_2O_3 at both intergranular and intragranular locations (see Fig. B2). Grain size analysis of the composite samples revealed a reduction in the average grain size of the matrix with the greatest reduction observed in samples containing the largest volume percent of submicron size Al_2O_3 (see Table B5). The average grain size increased with a reduction in volume percentage of submicron size Al_2O_3 indicating a superior ability of submicron

rather than nano-size Al_2O_3 particulates to inhibit grain growth. When compared to monolithic magnesium, the reduced grain size exhibited by the composite samples can primarily be attributed to the presence of reinforcement particulates and their ability to pin grain boundaries during sintering and hot extrusion steps.

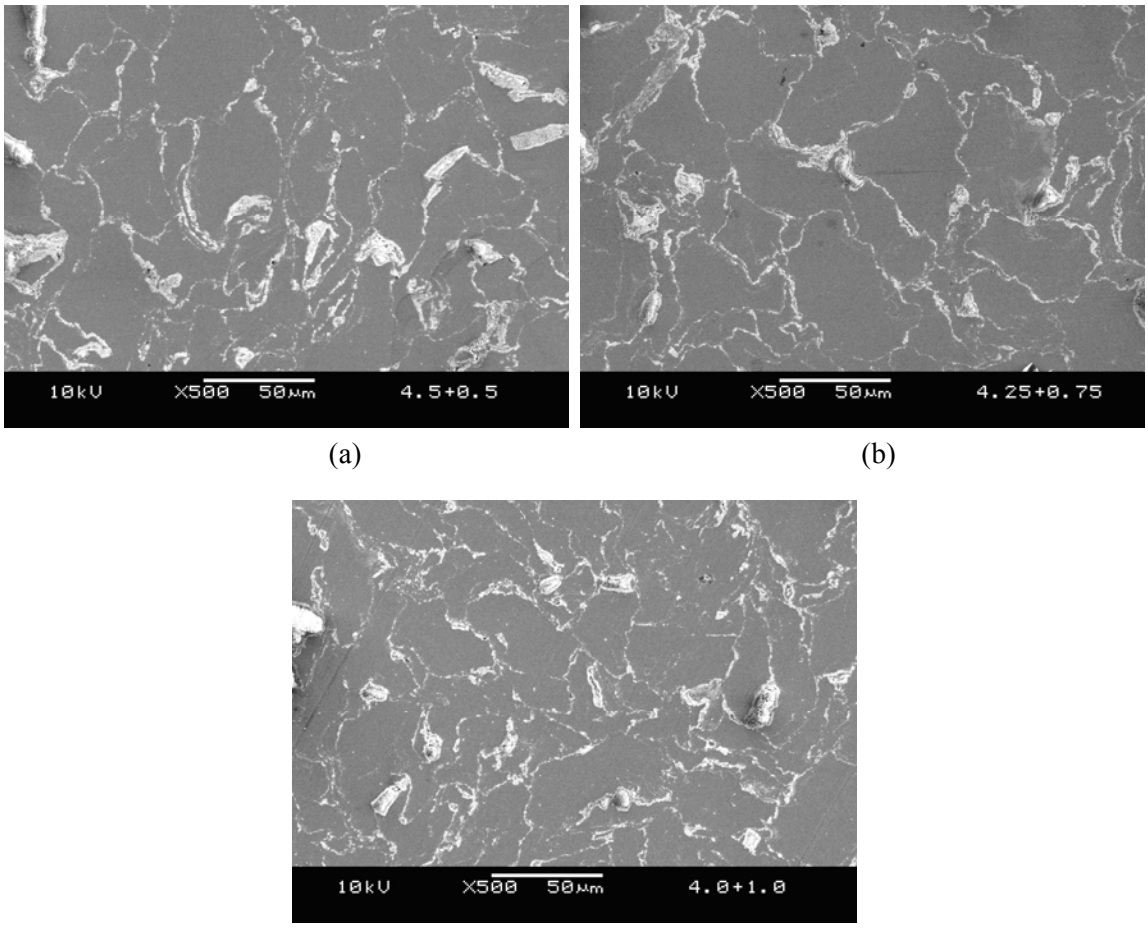

(a) (b)

(c)

Figure B2 Representative SEM micrographs showing the microstructures of: (a) Mg/ 4.5% (0.3-µm Al_2O_3)/0.5% (50-nm Al_2O_3), (b) Mg/ 4.25% (0.3-µm Al_2O_3)/0.75% (50-nm Al_2O_3), (c) Mg/ 4% (0.3-µm Al_2O_3)/1.0% (50-nm Al_2O_3).

Table B5 Results of grain size study and CTE measurements.

Materials	Reinforcement (Vol. %)		Grain Size (µm)	Aspect Ratio	CTE x 10^{-6}/°C
	50-nm	0.3-µm			
Mg	-	-	36 ± 4	1.68 ± 0.45	28.6 ± 0.8
Mg/ Al_2O_3	0.5	4.5	24 ± 8	2.26 ± 0.91	27.2 ± 1.2
Mg/ Al_2O_3	0.75	4.25	27 ± 9	1.83 ± 0.51	25.7 ± 0.6
Mg/ Al_2O_3	1.0	4.0	31 ± 7	1.65 ± 0.42	25.8 ± 0.8

B3.1.3 Thermomechanical Analysis

The results of CTE measurements in the temperature range of 50 – 400°C revealed that the coupled addition of submicron and nano sized Al_2O_3 reinforcements led to a reduction in the coefficient of thermal expansion values of the magnesium matrix (see Table B5). The reduction in CTE values can be attributed to the presence of submicron and nano-Al_2O_3 reinforcements which exhibit a lower CTE value of 7.0 x 10^{-6}/°C [1] when compared to pure magnesium (28.6 x 10^{-6}/°C) and the ability of the reinforcements to effectively constraint the expansion of the matrix. Within the hybrid composites, the formulations containing 0.75-1% nano size Al_2O_3 appeared to give best results.

Theoretical CTE values were computed for the Mg/Al_2O_3 composite formulations using the Rule of Mixtures (upper bound, Eq. B1), Turner's model (lower bound, Eq. B2) and Kerner's model (Eq. B3) [3] for comparison purposes using values provided in Table B8. The equations can be represented as:

$$\alpha_{comp} = \alpha_m V_m + \alpha_r V_r \tag{B1}$$

$$\alpha_{comp} = (\alpha_m V_m K_m + \alpha_r V_r K_r)/(V_m K_m + V_r K_r) \tag{B2}$$

$$\alpha_{comp} = \alpha_m - V_r(\alpha_m - \alpha_r)\ x\ \frac{K_m(3K_r + 4G_m)^2 + (K_r - K_m)(16G_m^2 + 12G_m K_r)}{(4G_m + 3K_r)[4V_r G_m(K_r - K_m) + 3K_r K_m + 4G_m K_m]} \tag{B3}$$

where, α, V, K, and G represents coefficient of thermal expansion, volume fraction, bulk modulus and shear modulus of the phase while the subscript m and r refer to the matrix and reinforcement, respectively. The experimental and computed values of the coefficient of thermal expansion for the Mg/Al_2O_3 composite formulations are shown in Fig. B3. It is observed that: (i) the experimental values lie between the theoretical values predicted using Kerner's and Turner's models and (ii) the experimental CTE values are close to

that predicted by Kerner's model for magnesium composite containing 0.5% nano-size Al_2O_3 and increasing volume percentage of nano-size Al_2O_3 particulates from 0.75 to 1.0% causes the CTE values to deviate further from the Kerner's model. In related studies, investigators reported that the CTE values of ZK60A magnesium alloy reinforced with particulate SiC and particulate B_4C reinforcements follow closely the Kerner's prediction [11]. The lower experimental values when compared to the Kerner's predictions indicate good realization of physical properties of the reinforcement and can be attributed to the coupled influence of: i) reasonably uniform distribution of submicron and nano-sized Al_2O_3 particulates, and ii) good interfacial integrity between Al_2O_3 particulates and the magnesium matrix. The significant deviation of CTE values of hybrid Mg-composites containing 0.75-1 vol% nano-Al_2O_3 from Kerner's prediction suggest the superior ability of Al_2O_3 in nano-length scale to control the dimensional stability of magnesium.

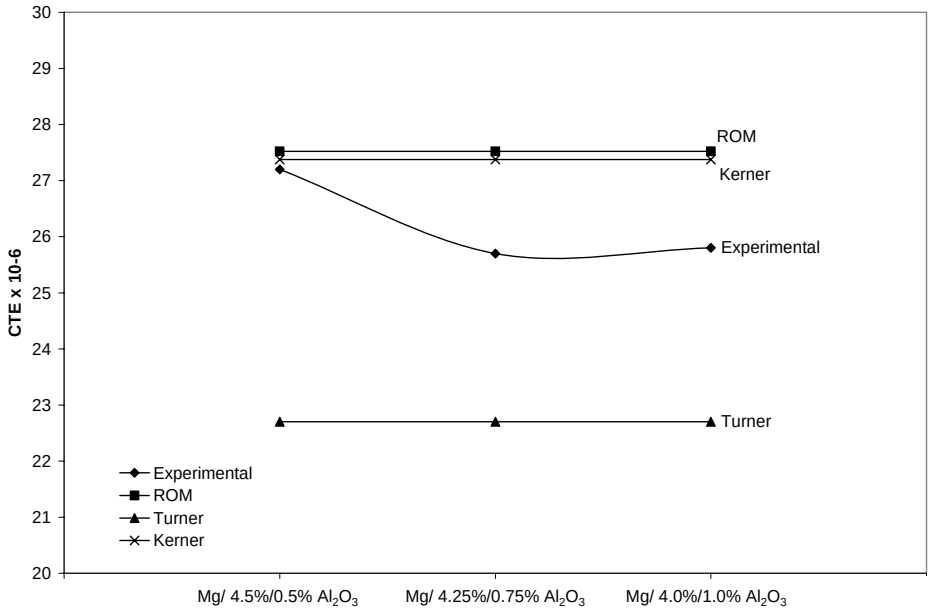

Figure B3 Graphical representation showing the experimental and theoretical CTE values.

B3.1.4 X-ray Diffraction Studies

The X-ray diffraction results corresponding to the Mg and hybrid Mg/Al_2O_3 samples were analyzed and the results of the phase analysis are shown in Table B6.

Table B6 Results of X-ray diffraction studies and microhardness measurements.

Materials	Reinforcement (Vol. %)		No. of matching peaks		Microhardness
	50-nm	0.3-μm	Mg	Al_2O_3	(HV)
Mg	-	-	6[1]	-	47.0 ± 1.3
Mg/ Al_2O_3	0.5	4.5	6[1]	4[1]	56.6 ± 1.2
Mg/ Al_2O_3	0.75	4.25	6[1]	4[1]	86.7 ± 1.7
Mg/ Al_2O_3	1.0	4.0	6[1]	4[1]	73.7 ± 1.1

[ ] represents the number of main peaks matched

B3.1.5 Mechanical Characterization

The results of microhardness measurements showed a marked increase in matrix hardness values in the case of hybrid magnesium composites (see Table B6). The increase in microhardness can be attributed to the presence of relatively harder Al_2O_3 particulates as reinforcements, which acts as a constraint to localized matrix deformation during indentation and the reduction in grain size (see Table B5). Amongst the hybrid composite formulations, the formulation with 0.75% nano-size Al_2O_3 exhibited the best microhardness value.

Tensile testing of the extruded specimens indicated an increase in elastic modulus, 0.2% yield strength and ultimate tensile strength of the hybrid composites and a reduction in ductility when compared to monolithic magnesium (see Table B7). Amongst the hybrid composites, the following trend was observed (see Table B7): i) an increase in elastic modulus and ductility with no apparent change in the strength of the hybrid composites upon the addition of nano-size alumina particulates between 0.5 to 0.75 volume percent, (ii) with an increase in the nano-size alumina particulates from 0.75 to 1

volume percentage, the overall mechanical properties of the hybrid composites were enhanced with an increase being observed in the elastic modulus, 0.2% yield strength, UTS and ductility of the composites.

Table B7 Results of room temperature tensile properties.

Materials	Reinforcement (Vol %) (Submicron)	(Nano)	E (GPa)	0.2%YS (MPa)	UTS (MPa)	Ductility (%)
Mg	-	-	45.0	116 ± 11.1	168 ± 10	9.0 ± 0.3
Mg/ Al_2O_3	4.5	0.5	50.5	139 ± 26.5	187 ± 28	1.9 ± 0.2
Mg/ Al_2O_3	4.25	0.75	51.9	138 ± 13.2	189 ± 15	2.4 ± 0.6
Mg/ Al_2O_3	4.0	1.0	54.4	157 ± 20.3	211 ± 21	3.0 ± 0.3
Mg/ SiC_p[1]	10	-	45	120	160	2
AZ91/SiC[2]	10	-	44.7	135	152	0.8
Mg/21.3 SiC[3]	21.3	-	50.0	128 ± 1.9	176 ± 3.5	1.4 ± 0.1
Mg/SiC/Al_2O_3. SiO_2[4]	8	-	53.4	-	201.3	2.13

[1] Data obtained from Ref. 16.
[2] Data obtained from Ref 2.
[3] Data obtained from Ref. 3.
[4] Data obtained from Ref. 17.

Elastic modulus measurements revealed that the coupled addition of submicron and nano-size Al_2O_3 leads to an increase in the elastic modulus of the magnesium matrix. The results further revealed that an increase in the relative proportion of nanosize Al_2O_3 particulates were more instrumental in increasing the elastic modulus of magenesium when compared to submicron size particulates (see Table B7). The results are consistent with the similar observation made on conventional Mg/Al_2O_3 nanocomposites [10]. The increase in elastic modulus of composite samples can be attributed to the presence of high modulus reinforcement ($E_{alumina}$ = 416 GPa [12]). Theoretical values for the elastic modulus were computed using the Rule of Mixtures [13] (Upper bound, Eq. B4a), lower bound (Eq. B4b) and Halpin-Tsai equation [1, 13] (Eq. 5a and 5b) using the values provided in Table B8:

$$E_c = V_m E_m + V_r E_r \tag{B4a}$$

$$E_c = E_m \left[\frac{E_m V_m + E_r (V_r + 1)}{E_r V_m + E_m (V_r + 1)} \right] \tag{B4b}$$

$$E_c = \frac{E_m (1 + 2sqV_r)}{1 - qV_r} \tag{B5a}$$

$$q = \frac{E_r / E_m - 1}{E_r / E_m + 2s} \tag{B5b}$$

where, E represents elastic modulus, s represents the aspect ratio of reinforcing phase and the subscripts c, m and r refer to the composite, matrix and reinforcement, respectively.

The experimental and theoretical values for the elastic modulus are shown in Fig. B4. The results show that the experimental values lie within the upper bound and Halpin-Tsai values. The experimental values remained superior when compared to Halpin-Tsai predictions indicating the superior ability of hybrid reinforcement to enhance elastic modulus when compared to the micron size reinforcement [3]. The experimental values obtained should still be considered lower-bound due to the presence of porosity. A model [14] was proposed recently that correlate the elastic modulus of the porous material (E) with the elastic modulus of the fully dense material (E_0) and the volume fraction of pores (p) through the following equations:

$$E = E_0 (1 - p^{2/3})^{1.21s} \tag{B6a}$$

$$s = (z/x)^{1/3} \left\{ 1 + \left[(z/x)^{-2} - 1 \right] \cos^2 \alpha_d \right\}^{1/2} \tag{B6b}$$

where z/x is the aspect ratio of the pores and α_d represents the relative orientation of the pores with respect to stress axis. The orientation factor $\cos^2\alpha_d$ is equivalent to 0.31 for a material with random orientation of pores which correspond to α_d of 56° [15]. Assuming

z/x = 1, the corrected elastic modulus was computed and is shown in Fig. B4. The results indicate an upward correction indicating the achievable modulus from the hybrid composites synthesized in the present study.

The increase in 0.2%YS of the hybrid composites when compared to pure magnesium can be attributed to: i) the Orowan strengthening mechanism triggered by nano-sized Al_2O_3 particulates, ii) decease in grain size, and iii) increase in dislocation density around the particulates due to different thermal expansion behavior of the matrix and particulates. An improvement of ~35% in 0.2%YS and ~26% in UTS over that of pure magnesium was achieved with the addition of 4 vol% submicron and 1 vol% nano-size Al_2O_3 particulates. The addition of Al_2O_3 particulates led to a reduction in the ductility of the magnesium matrix. However, it was observed that within hybrid composites increasing addition of nano-size Al_2O_3 particulates led to an increase in ductility. The increase in ductility observed with increasing volume percentage of nano-size Al_2O_3 particulates in the case of magnesium is consistent with the findings reported elsewhere [10].

It may be noted that the overall combination of mechanical properties exhibited by hybrid composite formulations synthesized in this study is found to be superior when compared to conventional Mg-based composites containing higher volume fraction of reinforcement and synthesized using other processing routes [2, 3, 16, 17] (see Table B7). This also establishes the feasibility of the microwave assisted 2-directional sintering technique used in this study to synthesize hybrid Mg/Al_2O_3 composite formulations with improved mechanical properties.

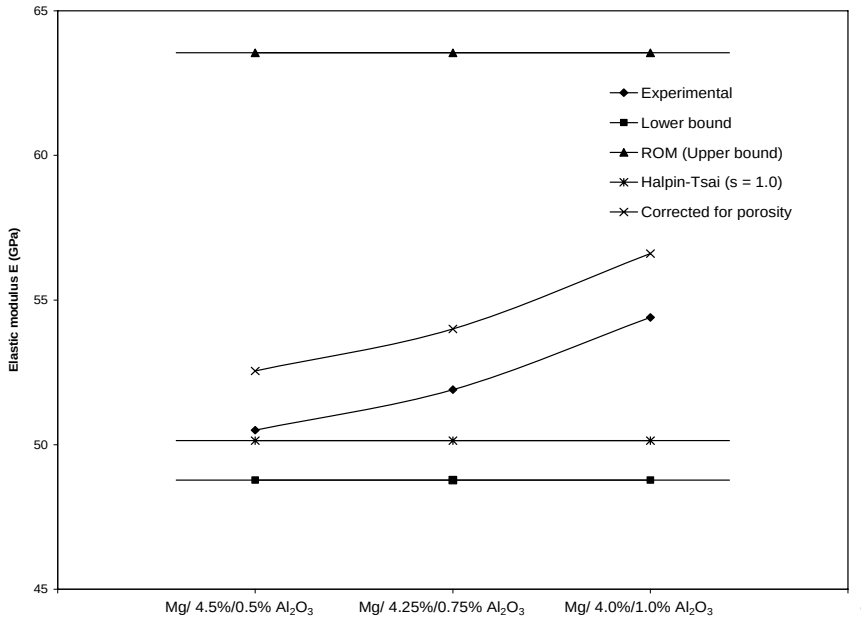

Figure B4 Graphical representation showing the experimental and theoretical modulus values.

Table B8 Properties of magnesium and alumina.

Materials	CTE X 10^{-6}	Elastic modulus (GPa)	Bulk modulus (GPa)	Shear Modulus (GPa)
Mg	28.6[1]	45[1]	36[2]	17.7[2]
Al_2O_3	7.0[3]	416[4]	257[4]	169[4]

[1] Data obtained from this study.
[2] Data obtained from Ref. 18.
[3] Data obtained from Ref. 1.
[4] Data obtained from Ref. 12.

B3.1.6 Fracture Behavior

The results of fracture surface analysis revealed predominance of cleavage steps in Mg samples (see Fig. B5). The presence of brittle cleavage steps can be attributed to the HCP crystal structure of magnesium that restricts the slip to the basal plane. The presence of cleavage steps and microscopically rough fracture surface indicates the inability of magnesium to deform significantly under uniaxial tensile loading. For the hybrid composite formulations, the fracture surface revealed not so well defined and prominent cleavage steps with increasing amount of nano-size Al_2O_3 particulates (see Fig. B5). This

can be attributed to particle damage during tensile loading and subsequent initiation and propagation of cracks along different paths. In related studies [3], investigators have convincingly shown that the presence of ceramic particulates such as SiC lead to formation of cracks in SiC/Mg interfacial region even in the absence of tensile loads. Further work is continuing in this area.

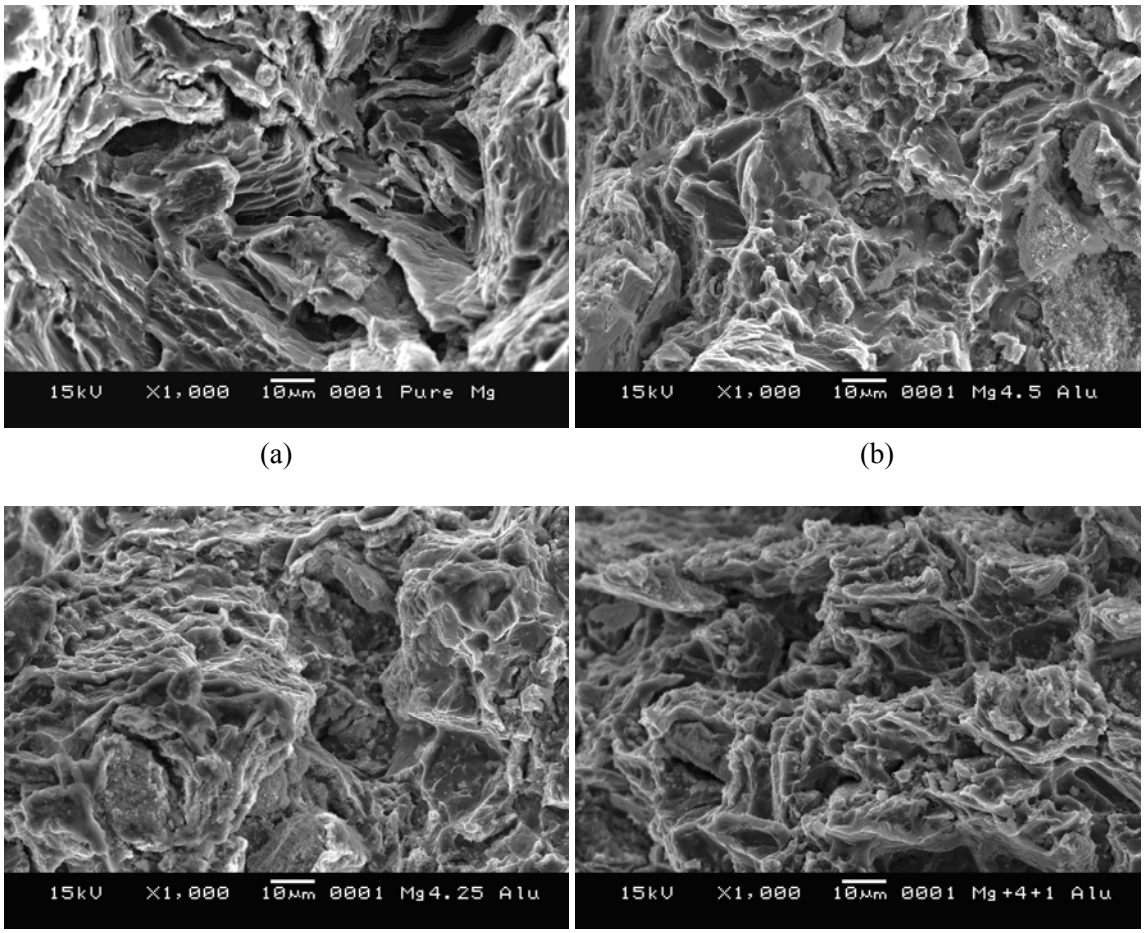

(a) (b)

(c) (d)

Figure B5 Representative SEM micrographs taken from the tensile fracture surface of: (a) Pure Mg, (b) Mg/ 4.5% (0.3-µm Al_2O_3)/0.5% (50-nm Al_2O_3), (c) Mg/ 4.25% (0.3-µm Al_2O_3)/0.75% (50-nm Al_2O_3), (d) Mg/ 4% (0.3-µm Al_2O_3)/1.0% (50-nm Al_2O_3).

B3.2 Conclusions

The following conclusions may be made from the results obtained in the present research investigation:

1. Powder metallurgy technique involving rapid microwave assisted 2-directional sintering and coupled with hot extrusion can be used to synthesize hybrid magnesium composites containing submicron and nano-Al_2O_3 particulates as reinforcements.
2. Results of coefficient of thermal expansion measurement indicate that the coupled addition of submicron and nano-Al_2O_3 reinforcements is able to improve the dimensional stability of magnesium matrix.
3. The coupled addition of submicron and nano-sized alumina reinforcements led to a significant increase in hardness, elastic modulus, yield strength and ultimate tensile strength but decreases the ductility of the composite formulations when compared to pure magnesium.
4. With an increase in the volume percent of nano-sized Al_2O_3 reinforcement from 0.75 to 1.0, the overall mechanical properties of the composites were enhanced with an increase being observed in elastic modulus, 0.2% yield strength, UTS and ductility of the composites.

References

1. D.J. Lloyd. Int Mater Rev 39: 1-23. 1994.
2. A. Luo. Metall Mater Trans A 26: 2445-2455. 1995.
3. M. Gupta, M.O. Lai, D. Saravanarangathan. J Mater Sci 35: 2155-2165. 2000.
4. J. Schröder and K.U. Kainer. Mat Sci Eng A 135: p.33. 1991.
5. I. Park, I. Choi and K. Cho. Mater Sci Forum 449-452: p.653. 2004.

6. B.W. Chua, L. Lu and M.O. Lai. Comp Struct 47: 595-601. (1999)

7. S.R. Agnew, O. Duygulu. Int J Plast 21: 1161-1193. 2005.

8. S.F. Hassan, M. Gupta. J Alloy Compd 345: 246-251. 2002.

9. C.S. Goh, J. Wei, L.C. Lee, M. Gupta, Nanotechnology 17: 7-12. 2006.

10. S.F. Hassan, M. Gupta. Mat Sci Eng A 392: 163-168. 2005.

11. A.L. Geiger and M. Jackson, Adv Mat Proc 136(7): p. 23. 1989.

12. Website: http://www.ceramics.nist.gov/srd/summary/scdaos.htm, last accessed Oct 2004.

13. M.Gupta and M.K. Surappa, Key Eng Mater 104-107: p. 259. 1995.

14. A.R. Boccacini, G. Ondracek, P. Mazilu and D. Windelbeg. J Mech Behav Mater 4: p. 119. 1993.

15. G.E. Fougere, L. Riester, M. Ferber, J.R. Weertman and R.W. Siegel, Mat Sci Eng A – Struct 204: 1-6. 1995.

16. M.R. Krishnadev, R. Angers, C.G. Krishnadas Nair, G. Huard. JOM 45: 52-54. 1993.

17. X. N. Zhang, R.J. Wu. Key Eng Mater 249: p. 217. 2003.

18. A. Buch. Pure Metals Properties. Materials Park, Ohio, USA: ASM International. p.20. 1999.